

Yarkovsky–O’Keefe–Radzievskii–Paddack effect with anisotropic radiation

S. Breiter¹* and D. Vokrouhlický²*

¹*Astronomical Observatory, A. Mickiewicz University, Słoneczna 36, PL60-286 Poznań, Poland*

²*Institute of Astronomy, Charles University, V Holešovičkách 2, 18000 Prague 8, Czech Republic*

Accepted 2010 September 7. Received 2010 September 4; in original form 2010 July 21

ABSTRACT

In this paper, we study the influence of optical scattering and thermal radiation models on the Yarkovsky–O’Keefe–Radzievskii–Paddack (YORP) effect. The Lambertian formulation is compared with the scattering and emission laws and Lommel–Seeliger reflection. Although the form of the reflectivity function strongly influences the mean torques because of scattering or thermal radiation alone, their combined contribution to the rotation period YORP effect is not very different from the standard Lambertian values. For higher albedo values, the differences between the Hapke and Lambert models become significant for the YORP effect in attitude.

Key words: radiation mechanisms: thermal – methods: numerical – celestial mechanics – minor planets, asteroids: general.

1 INTRODUCTION

Over the last decade, the importance of radiation recoil forces on both orbital motion and the rotation of minor bodies in the Solar system has been widely appreciated. The Yarkovsky effect, caused by lagged thermal radiation from the surface of a spinning body – directly detected in the orbital motion of (6489) Golevka (Chesley et al. 2003) and 1992 BF (Vokrouhlický, Chesley & Matson 2008) – has been the key to a proper understanding of asteroid long-term dynamics. Since the paper of Rubincam (2000), the influence of torques as a result of radiation recoil has been known as the Yarkovsky–O’Keefe–Radzievskii–Paddack (YORP) effect, acknowledging the works of Yarkovsky (1901), Radzievskii (1954), Paddack (1969) and O’Keefe (1976). Unlike the orbital Yarkovsky effect, the YORP effect involves both the scattering of incident light and its thermal reradiation, and it occurs even for objects with zero conductivity. Direct detections of the YORP effect in the rotation of asteroids (54509) YORP (Lowry et al. 2007; Taylor et al. 2007), (1862) Apollo (Kaasalainen et al. 2007), (1620) Geographos (Ďurech et al. 2008b) and (3103) Eger (Ďurech et al. 2009) have proved the existence of the YORP effect. However, the agreement between the observed and modelled values in each case can be qualified as merely having a similar order of magnitude, and all present YORP models are still simplified and incomplete. What is worse, the failure to detect a theoretically predicted YORP effect for (25143) Itokawa (Ďurech et al. 2008a) has helped us to realize that these simplified models have an extreme sensitivity to the fine details of shape, centre of mass location and spin axis orientation in the body frame (Ďurech et al. 2008a; Scheeres & Gaskell 2008;

Statler 2009; Breiter et al. 2009). On the other hand, direct radiation pressure has no effect on the mean torque, regardless of the shape, as observed by Rubincam (2000) and proved by Nesvorný & Vokrouhlický (2008) and Rubincam & Paddack (2010).

Most of these models assume that both scattering and thermal radiation are Lambertian (i.e. a photon can be emitted or scattered with equal probability in any direction, and hence the exiting flux is proportional to the cosine of zenith distance according to the projected area of the radiating/scattering surface element). Although Breiter et al. (2007) and Scheeres (2007) mentioned a more general scattering model, their subsequent works on the YORP effect were actually based upon the Lambertian assumption. Statler (2009) took a step further, using a hemispheric albedo derived from the scattering model of Hapke (2002) instead of the usual Bond albedo (Vokrouhlický & Bottke 2001). Moreover, the TACO model of Statler for the first time incorporates the important observation that photons bouncing between various surface elements do not produce net torque until they finally exit into outer space.

The main objective of the present work is to include non-Lambertian scattering and radiation into the recent YORP model of Breiter, Bartczak & Czekaj (2010) and to judge the significance of this improvement. Roughly speaking, a departure from the Lambertian model is essentially caused by inter-reflections and occlusions. Both phenomena occur at various levels of resolution and we have to be careful about this issue. Out of the two principal scattering models for asteroid surfaces developed by Lumme & Bowell (1981) and Hapke (Hapke 1981, 1984, 1986, 2002, 2008; Hapke & Wells 1981), we have chosen the latter. However, both models were created to interpret photometric observations; as such, they attempt to include phenomena occurring at various resolution levels that merge in the final integrated brightness. In these circumstances, in this paper we focus on accounting for the regolith grain-size-scale

*E-mail: breiter@amu.edu.pl (SB); vokrouhl@cesnet.cz (DV)

(<1 mm) phenomena described by an appropriate part of the Hapke reflectance and emissivity models. This means ignoring the macroscopic roughness corrections and shape-dependent beaming factors. Inter-reflections occurring between larger surface fragments require a different approach and will be discussed in another paper, whereas the large-scale occlusions (shadowing) are already incorporated in most existing YORP models. To a large extent, the present contribution has been motivated by the problem of the YORP effect on a high albedo asteroid (3103) Eger, where only a convex shape model is available, so larger-scale inter-reflections have to be neglected anyway.

We have decided to present a detailed derivation of the radiation recoil force and associated YORP torque using the terminology of modern radiometry instead of the traditional astrophysical framework dating back to Chandrasekhar (1950). In this respect, we owe much to the collection of Max Fairbairn essays available on-line thanks to J. B. Tatum.¹

2 SCATTERING AND RADIATION

2.1 Irradiance

Consider an infinitesimal element dS of the surface of a celestial body without an atmosphere. Further, we call dS a physical surface, to distinguish it from a normal surface (i.e. an infinitesimal surface perpendicular to some specified direction of incident or emitted radiation).

The local solar frame (LSF) is defined with the origin at the centre of dS , with the x -axis pointing to the intersection of the meridian passing through the Sun and the horizon plane, with the z -axis directed along the outward normal to the physical surface (i.e. to the local zenith) and with the y -axis completing the right-handed orthogonal system. Then, the unit vector directed to the Sun has a simple form

$$\mathbf{s} = \begin{pmatrix} s_{\odot} \\ 0 \\ \mu_{\odot} \end{pmatrix}, \quad (1)$$

depending only on the solar zenith distance through its cosine μ_{\odot} and sine

$$s_{\odot} = \sqrt{1 - \mu_{\odot}^2}. \quad (2)$$

If the Sun is located at the distance R_{\odot} , the collimated radiation flux density (power per normal area perpendicular to \mathbf{s}) arriving from the point R_{\odot} \mathbf{s} is

$$J = J_0 \left(\frac{R_0}{R_{\odot}} \right)^2, \quad (3)$$

where the solar constant $J_0 \approx 1366 \text{ W m}^{-2}$ is defined for a nominal distance $R_0 = 1 \text{ au}$. The irradiance or insolation E of an arbitrarily oriented surface element is the ratio of the incident power flux $d\Phi_i$ to the physical area dS . Accounting for the area projection factor $\mathbf{s} \cdot \mathbf{n} = \mu_{\odot}$, where \mathbf{n} is the unit vector directed to zenith, we can write

$$E(\mathbf{s}) = \frac{d\Phi_i}{dS} = \nu J \mu_{\odot}. \quad (4)$$

The visibility function ν is either 1, when the Sun is visible at dS , or 0, when the Sun is occluded.

2.2 Bidirectional scattering

The incident radiant power $d\Phi_i = E dS$ is partially absorbed (converted into heat) and partially reflected in various directions \mathbf{o}

$$\mathbf{o} = \begin{pmatrix} \sqrt{1 - \mu^2} \cos \phi \\ \sqrt{1 - \mu^2} \sin \phi \\ \mu \end{pmatrix}, \quad (5)$$

where μ is the cosine of the zenith distance and ϕ is the azimuth angle in the LSF. The cosine of the phase angle between \mathbf{s} and \mathbf{o} is designated as μ' , and defined as the scalar product

$$\mu' = \mathbf{s} \cdot \mathbf{o} = s_{\odot} \sqrt{1 - \mu^2} \cos \phi + \mu_{\odot} \mu. \quad (6)$$

The power flux $d^2\Phi_r$ scattered from dS into a solid angle $d\Omega$ in the direction \mathbf{o} is described by the reflected radiance L_r

$$L_r(\mathbf{o}) = \frac{d^2\Phi_r}{\mu dS d\Omega}, \quad (7)$$

where μdS is the normal surface perpendicular to \mathbf{o} . Writing $L_r(\mathbf{o})$, we should bear in mind an implicit dependence on the direction of the Sun \mathbf{s} , because the reflected power also depends on the incident flux from the Sun. This dependence becomes more explicit when we introduce a bidirectional reflectance distribution function (BRDF) f_r , defined as the ratio of the radiance L_r reflected in the direction \mathbf{o} to the irradiance E from the energy source located in the direction \mathbf{s} :

$$f_r(\mathbf{s}, \mathbf{o}) = \frac{L_r(\mathbf{o})}{E(\mathbf{s})}. \quad (8)$$

Although a bidirectional reflectance (BDR) function ρ

$$\rho(\mathbf{s}, \mathbf{o}) = \mu_{\odot} f_r(\mathbf{s}, \mathbf{o}), \quad (9)$$

seems to be more common in planetary photometry than the BRDF, we choose f_r as a more convenient quantity offering, for example, the reciprocity relation $f_r(\mathbf{s}, \mathbf{o}) = f_r(\mathbf{o}, \mathbf{s})$. Using equation (8) we can express the reflected radiance as

$$L_r(\mathbf{o}) = f_r(\mathbf{s}, \mathbf{o}) E(\mathbf{s}) = \nu f_r(\mathbf{s}, \mathbf{o}) \mu_{\odot} J. \quad (10)$$

Recalling, for reference, a traditional, Lambertian BRDF with albedo A

$$f_L = \frac{A}{\pi}, \quad (11)$$

we adopt the anisotropic BRDF proposed by Hapke, namely its version from Hapke (2002) without macroscopic roughness effects:

$$f_r(\mathbf{s}, \mathbf{o}) = \frac{w}{4\pi(\mu_{\odot} + \mu)} [(1 + B)P + H(\mu_{\odot})H(\mu) - 1]. \quad (12)$$

Here, the Henyey–Greenstein particle phase function is

$$P = (1 - g^2)[1 + 2g\mu' + g^2]^{-3/2}, \quad (13)$$

and the opposition surge function B is defined as

$$B = B_0 \left[1 + \frac{1}{h} \sqrt{\frac{1 + \mu'}{1 - \mu'}} \right]^{-1}, \quad (14)$$

with

$$B_0 = \frac{S_0 (1 + g)^2}{w (1 - g)}. \quad (15)$$

The Chandrasekhar multiple scattering function H is defined in terms of an integral equation (Chandrasekhar 1950), but we use the explicit second-order approximation given by Hapke (2002)

$$H(x) = \left[1 - wx \left(r_0 + \frac{1 - 2r_0x}{2} \ln \frac{1 + x}{x} \right) \right]^{-1}, \quad (16)$$

¹ <http://orca.phys.uvic.ca/tatum/plphot.html>

where

$$r_0 = \frac{1 - \sqrt{1-w}}{1 + \sqrt{1-w}}. \quad (17)$$

Thus, apart from the incoming and scattered flux directions s and \mathbf{o} , the Hapke BRDF depends on four physical parameters of the surface: the single scattering albedo w , the regolith compaction parameter h , the opposition surge amplitude S_0 (sometimes replaced by B_0) and the asymmetry factor of the Henyey–Greenstein function g . A more recent version of reflectance was proposed by Hapke (2008); the modification amounts to adding the dependence on porosity as a multiplicative factor in f_r and a divisor in the argument of H . This modification is easy to implement, but we suspend its use until controversies concerning the dependence of the opposition effect on porosity are resolved (Hapke 2008).

The total power flux Φ_e emitted into the hemisphere

$$\Omega_+ = \{(\mu, \phi) : 0 \leq \mu \leq 1, 0 \leq \phi < 2\pi\},$$

divided by the emitting physical area is called the radiant exitance M

$$M = \frac{d\Phi_e}{dS}. \quad (18)$$

Recalling definition (7), we find for the exitance as a result of scattering

$$M_r = \int_{\Omega_+} \frac{d^2\Phi_r}{dS d\Omega} d\Omega = \int_{\Omega_+} L_r(\mathbf{o}, s) \mu d\Omega. \quad (19)$$

However, according to equation (8), radiance is related to irradiance by the BRDF f_r , and hence

$$M_r(s) = E(s) \int_{\Omega_+} f_r(s, \mathbf{o}) \mu d\Omega, \quad (20)$$

and the dependence on the Sun's location s appears explicitly.

At this point, we can introduce the notion of hemispheric albedo A_h as the ratio

$$A_h(\mu_\odot) = \frac{M_r}{E(s)}. \quad (21)$$

Combining equations (20) and (21), we see that

$$A_h(\mu_\odot) = \int_{\Omega_+} f_r(s, \mathbf{o}) \mu d\Omega = \int_0^{2\pi} d\phi \int_0^1 f_r(s, \mathbf{o}) \mu d\mu, \quad (22)$$

and equation (20) is simplified to

$$M_r(s) = E(s) A_h(\mu_\odot). \quad (23)$$

For a given set of Hapke parameters, the integral (22) can be evaluated numerically on a sufficiently dense set of μ_\odot values, allowing us to construct an appropriate approximating function. Using the least-squares adjustment, we construct

$$\mu_\odot A_h(\mu_\odot) \approx A_B \mu_\odot + \alpha_1 \mu_\odot \frac{1 - \alpha_2 \mu_\odot}{1 + \alpha_3 \mu_\odot}, \quad (24)$$

where the Bond albedo A_B , defined as

$$A_B = \frac{1}{\pi} \int_{\Omega_+} A_h(\mu_\odot) \mu_\odot d\Omega_\odot = 2 \int_0^1 A_h(\mu_\odot) \mu_\odot d\mu_\odot, \quad (25)$$

is the mean slope of the product $\mu_\odot A_h$, and the coefficients α_i of a simple rational approximation describe the deviation from the linear model. We focus on the properties of $\mu_\odot A_h$, because in the following sections the hemispheric albedo always appears multiplied by the cosine of the Sun's zenith distance. Note that the adjustment of $A_h(\mu_\odot)$ leads to different values of α_i , degrading the quality of approximation of the product $\mu_\odot A_h$.

2.3 Geometric albedo

Although the geometric (or physical) albedo is not directly involved in the computation of the radiation recoil force, we need it to select an appropriate value of w for the Hapke model, because usually the observations provide only the geometric albedo and the spectral type for an asteroid.

Let us begin with the notion of intensity I . In contrast to the previously discussed quantities, the intensity refers to the power $d\Phi$ emitted from the surface of the whole body (not only from an infinitesimal dS) in some direction \hat{q} , divided by the solid angle $d\Omega$ centred at \hat{q} :

$$I(\hat{q}) = \frac{d\Phi}{d\Omega}. \quad (26)$$

The geometric albedo p is the ratio of the observed intensity of some presumably spherical object to the intensity of the Lambertian disc with the same diameter as the assumed sphere – both observed in the direction of the Sun (i.e. with a zero phase angle). This leads to the integral definition

$$p = 2\pi \int_0^1 \mu_\odot^2 f_r(s, s) d\mu_\odot. \quad (27)$$

Verbiscer & Veverka (1995) provide expressions that allow us to compute Hapke parameters h , B_0 and g for various spectral types as functions of a given geometric albedo p and the mean slope parameter G of the International Astronomical Union (IAU) two-parameter magnitude system (Bowell et al. 1989).

2.4 Directional thermal emission

The energy leaving a surface element dS does not consist only of scattered radiation. If the element has temperature $T > 0$, it also emits thermal radiation. Radiant exitance M_b through Ω_+ for a blackbody is given by the Stefan–Boltzmann law:

$$M_b = \frac{d\Phi_b}{dS} = \sigma T^4. \quad (28)$$

Here, $\sigma = 5.67 \times 10^{-8} \text{ W m}^{-2} \text{ K}^{-4}$ is the Stefan–Boltzmann constant and Φ_b is the blackbody value of a more general thermal radiation power flux Φ_t . The point blackbody radiation is, by definition, isotropic whereas a blackbody surface radiation is Lambertian. So, the associated radiance $L_b(\mathbf{o})$ in the direction \mathbf{o} is obtained from the general definition of a thermally emitted radiance L_t analogous to equation (10)

$$L_t(\mathbf{o}) = \frac{d^2\Phi_t}{\mu dS d\Omega}, \quad (29)$$

dividing the exitance M_b by the ‘ μ -averaged’ solid angle of a hemisphere π :

$$L_b = \frac{M_b}{\pi}. \quad (30)$$

Indeed, using equation (30) and the definition of exitance, we verify that

$$\int_{\Omega_+} L_b \mu d\Omega = M_b. \quad (31)$$

The hemispheric emissivity ϵ_h is defined as the ratio of actual thermal exitance M_t to the blackbody exitance M_b

$$\epsilon_h = \frac{M_t}{M_b}. \quad (32)$$

This global quantity should not be confused with a directional emissivity $\epsilon(\mathbf{o})$, defined as the ratio of radiances

$$\epsilon(\mathbf{o}) = \frac{L_t(\mathbf{o})}{L_b(\mathbf{o})}. \quad (33)$$

Directional emissivity plays a role similar to that of the BRDF in scattering, although their definitions essentially differ: the former is the dimensionless ratio of two radiances, while the latter (with dimension sr^{-1}) is the ratio of radiance to irradiance. So, the thermally emitted radiance in the direction of \mathbf{o} can be expressed as

$$L_t(\mathbf{o}) = \epsilon(\mathbf{o})L_b(\mathbf{o}) = \frac{\epsilon(\mathbf{o})}{\pi}\sigma T^4. \quad (34)$$

In this paper, we adopt the directional emissivity function of Hapke (Hapke 1993; Lagerros 1996)

$$\epsilon(\mu) = \sqrt{1-w}H(\mu), \quad (35)$$

where w is the Hapke single scattering albedo, and the Chandrasekhar function H is given by equation (16). Thus, the emitted radiance is

$$L_t(\mathbf{o}) = \epsilon(\mu)\frac{\sigma T^4}{\pi} = \frac{\sqrt{1-w}}{\pi}H(\mu)\sigma T^4. \quad (36)$$

The exitance M_t resulting from equation (36) is

$$M_t = \int_{\Omega_+} L_t(\mathbf{o})\mu \, d\Omega. \quad (37)$$

Comparing this with the primary definition of ϵ_h (equation 32), we can use the relation

$$M_t = \epsilon_h\sigma T^4. \quad (38)$$

This leads to the integral expression of hemispheric emissivity

$$\epsilon_h = \int_{\Omega_+} \frac{\epsilon(\mu)\mu}{\pi} \, d\Omega = 2 \int_0^1 \epsilon(\mu)\mu \, d\mu, \quad (39)$$

evaluating to a single number for a given set of Hapke parameters.

The infrared radiation of asteroids is often related to the notion of the beaming effect, empirically accounted for by the beaming factor η (Lebofsky & Spencer 1989; Lagerros 1996). We do not introduce the beaming factor in our model for a number of reasons, as follows. (i) The part of the beaming that depends on grain-size-scale radiation transfer should be present in the emissivity function of Hapke. (ii) The contribution of thermal lag to the beaming factor is present in the surface temperature model with conductivity. (iii) The larger-scale radiation exchange contribution (Lagerros 1998) will be included in future extensions of our model together with optical inter-reflections.

2.5 Energy balance

The conservation of energy implies that the total power scattered, thermally re-emitted and conducted inside the body should be equal to the incident power flux Φ_i . In terms of power density (per physical surface), this means that

$$E(\mathbf{s}) = M_r(\mathbf{s}) + M_t - Q, \quad (40)$$

that is, irradiance E is equal to the sum of total radiant exitance M and of the conducted heat flux density ($-Q$). Given a non-zero surface conductivity K , we have

$$Q = -K\mathbf{n} \cdot \nabla T, \quad (41)$$

and then

$$E(\mathbf{s}) = A_h(\mu_\odot)E(\mathbf{s}) + \epsilon_h\sigma T^4 + K\mathbf{n} \cdot \nabla T, \quad (42)$$

or

$$\epsilon_h\sigma T^4 = \nu\mu_\odot[1 - A_h(\mu_\odot)]J + Q. \quad (43)$$

If $K = 0$, equation (43) directly provides the surface temperature, generalizing the usual Lambertian Rubincam approximation of the YORP effect to the Hapke reflectance/emissivity model. With $K \neq 0$, equation (43) serves as a boundary condition for the heat conduction problem.

3 RADIATION RECOIL FORCE AND TORQUE

3.1 Force expression

The photon flux, leaving dS in the direction \mathbf{o} , carries energy and momentum (energy divided by the velocity of light c), inducing the recoil force \mathbf{F} equal to the time derivative of momentum and directed opposite to \mathbf{o} . The force can be easily expressed in terms of emitted radiance, provided we introduce a radiance vector

$$\mathbf{L}(\mathbf{o}) = L(\mathbf{o})\mathbf{o}, \quad (44)$$

where L is the sum of scattered L_r and thermal L_t . The definition of radiance implies that the force density in the direction \mathbf{o} per physical area and solid angle is

$$\frac{d^2\mathbf{F}}{dS \, d\Omega} = -\frac{d^2(\Phi_r + \Phi_t)}{dS \, d\Omega} \frac{\mathbf{o}}{c} = -\frac{\mu}{c}\mathbf{L}(\mathbf{o}). \quad (45)$$

Integrating over the hemisphere Ω_+ , we find the net force per physical area

$$\frac{d\mathbf{F}}{dS} = -\frac{1}{c} \int_{\Omega_+} \mu\mathbf{L}(\mathbf{o}) \, d\Omega. \quad (46)$$

Substituting equations (10) and (34), we have

$$\frac{d\mathbf{F}}{dS} = -\frac{1}{c} \int_{\Omega_+} \mu \left[f_r(\mathbf{s}, \mathbf{o})E(\mathbf{s}) + \frac{\epsilon(\mu)}{\pi}\sigma T^4 \right] \mathbf{o} \, d\Omega, \quad (47)$$

or, observing the independence of directional emissivity on azimuth,

$$\frac{d\mathbf{F}}{dS} = -\frac{E(\mathbf{s})}{c} \int_{\Omega_+} \mu f_r(\mathbf{s}, \mathbf{o})\mathbf{o} \, d\Omega - \frac{2\sigma T^4\mathbf{n}}{c} \int_0^1 \mu^2\epsilon(\mu) \, d\mu. \quad (48)$$

Using the LSF, we can conveniently decompose the force density into the sum of two perpendicular components along the axes z and x (i.e. along the surface normal \mathbf{n} and the unit vector \mathbf{m}):

$$\mathbf{n} = \begin{pmatrix} 0 \\ 0 \\ 1 \end{pmatrix}, \quad \mathbf{m} = \begin{pmatrix} 1 \\ 0 \\ 0 \end{pmatrix}. \quad (49)$$

In an arbitrary reference frame, we can compute \mathbf{m} as

$$\mathbf{m} = (\mathbf{s} - \mu_\odot\mathbf{n})s_\odot^{-1}, \quad (50)$$

taking $\mu_\odot = \mathbf{s} \cdot \mathbf{n}$.

Splitting the first integrand in equation (48) into a sum

$$\begin{aligned} \mu f_r(\mathbf{s}, \mathbf{o})\mathbf{o} &= f_r\mu^2\mathbf{n} + f_r\mu\sqrt{1-\mu^2}\cos\phi\mathbf{m} \\ &\quad + f_r\mu\sqrt{1-\mu^2}\sin\phi(\mathbf{n} \times \mathbf{m}), \end{aligned} \quad (51)$$

and recalling that $f_r(\mathbf{s}, \mathbf{o})$ is an even function of azimuth ϕ , and thus the last term in equation (51) is odd and its integral over Ω_+ does vanish, we introduce two auxiliary functions

$$I_1(\mu_\odot) = \int_0^{2\pi} d\phi \int_0^1 \mu^2 f_r(\mathbf{s}, \mathbf{o}) \, d\mu, \quad (52)$$

$$I_2(\mu_\odot) = \int_0^{2\pi} d\phi \int_0^1 \mu\sqrt{1-\mu^2}\cos\phi f_r(\mathbf{s}, \mathbf{o}) \, d\mu, \quad (53)$$

as well as a coefficient

$$I_3 = 2 \int_0^1 \mu^2 \epsilon(\mu) d\mu. \quad (54)$$

These allow us to rewrite equation (48) as

$$\frac{d\mathbf{F}}{dS} = -\frac{E(s)}{c} [I_1(\mu_\odot)\mathbf{n} + I_2(\mu_\odot)\mathbf{m}] - \frac{I_3\sigma T^4}{c}\mathbf{n}. \quad (55)$$

Substituting the boundary conditions (42) into equation (55), we remove the explicit dependence on T^4 , obtaining

$$\begin{aligned} \frac{d\mathbf{F}}{dS} = & -\frac{E(s)}{c} \left\{ \left[I_1(\mu_\odot) + I_3 \frac{1 - A_h(\mu_\odot)}{\epsilon_h} \right] \mathbf{n} + I_2(\mu_\odot)\mathbf{m} \right\} \\ & - \frac{Q I_3}{c\epsilon_h} \mathbf{n}. \end{aligned} \quad (56)$$

However, we prefer to rearrange the force expression into a more comprehensive form

$$\frac{d\mathbf{F}}{dS} = -\frac{2}{3} \frac{1 + \xi}{c} [vJ\mu_\odot + Q]\mathbf{n} + \frac{vJ}{c} [X_1\mathbf{n} - X_2\mathbf{m}], \quad (57)$$

where the function arguments have been omitted for the sake of brevity.

The coefficient

$$\xi = \frac{3}{2} \frac{I_3}{\epsilon_h} - 1 \quad (58)$$

is a small quantity of order 10^{-2} or less. The two functions

$$X_1 = \mu_\odot \left(\frac{A_h I_3}{\epsilon_h} - I_1 \right), \quad (59)$$

and

$$X_2 = \mu_\odot I_2, \quad (60)$$

also represent a small deviation from the Lambertian model (see Fig. 1, based upon the data from Table 1).

We believe that there is no point in producing excessively accurate approximations of corrections to the Lambertian model, so we use relatively simple functions, found by trial and error,

$$X_1 \approx \xi_{10} \mu_\odot \frac{1 - \mu_\odot - \xi_{11} \mu_\odot^2}{1 + 3\mu_\odot - \xi_{12} \mu_\odot^2}, \quad (61)$$

$$X_2 \approx \xi_{20} \mu_\odot \left(3 - \xi_{21} \mu_\odot + \mu_\odot^2 \right) \sqrt{\frac{1 - \mu_\odot}{1 + \mu_\odot}}, \quad (62)$$

with coefficients ξ_i generated by the least-squares adjustment to the results of numerical quadratures.

The limit case of the Lambertian model results from setting $\xi = X_1 = X_2 = 0$. Then, equation (57) simplifies to

$$\frac{d\mathbf{F}_L}{dS} = -\frac{2}{3c} (vJ\mu_\odot + Q)\mathbf{n}. \quad (63)$$

Of course, this step also requires the assumption of a constant $A_h = A_B$ in boundary conditions (42) for a heat conduction solver providing Q .

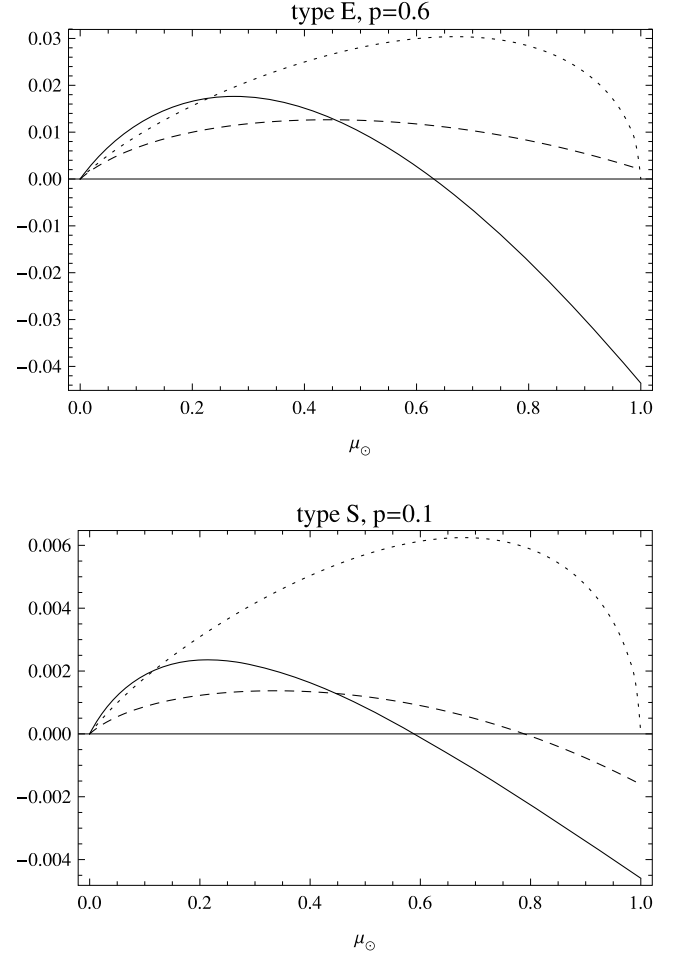


Figure 1. Functions describing the non-Lambertian force model. The solid line represents the remainder $\mu_\odot(A_h - A_B)$, and dashed and dotted lines refer to X_1 and X_2 , respectively.

3.2 Torque expression

The force defined by equation (57) generates for each surface element a torque:²

$$\begin{aligned} d\mathbf{M} = & \left(\mathbf{r} \times \frac{d\mathbf{F}}{dS} \right) dS = -\frac{2}{3} \frac{1 + \xi}{c} [vJ\mu_\odot + Q] (\mathbf{r} \times d\mathbf{S}) \\ & + \frac{vJ}{c} [X_1 (\mathbf{r} \times d\mathbf{S}) - X_2 (\mathbf{r} \times \mathbf{m} dS)]. \end{aligned} \quad (64)$$

The two cross products in this equation differ in nature: the first,

$$\mathbf{r} \times d\mathbf{S} = \mathbf{r} \times \mathbf{n} dS, \quad (65)$$

is constant over time in the body frame, whereas the second,

$$\begin{aligned} \mathbf{r} \times \mathbf{m} dS &= \frac{\mathbf{r} \times \mathbf{s} - \mu_\odot \mathbf{r} \times \mathbf{n}}{s_\odot} dS \\ &= \frac{\mathbf{r} \times \mathbf{s}}{s_\odot} dS - \frac{\mu_\odot}{s_\odot} (\mathbf{r} \times d\mathbf{S}), \end{aligned} \quad (66)$$

is time-dependent because of the solar motion on the local celestial sphere of dS .

² We maintain the symbol \mathbf{M} from previous papers, hoping that it will not be confused with exittance M appearing only in Section 2.

Table 1. Sample Hapke parameters and related quantities.

	$p = 0.6$, type E	$p = 0.1$, type S
w	0.856	0.139
h	0.044	0.049
B_0	0.8576	1.5407
g	-0.2459	-0.2593
A_B	0.47542	0.046712
α_1	0.14550	0.031021
α_2	1.5880	1.6968
α_3	0.9741	3.6800
ξ_{10}	0.09590	0.01212
ξ_{11}	-0.03374	0.3383
ξ_{12}	2.1268	1.4786
ξ_{20}	0.032156	0.006259
ξ_{21}	0.42458	0.16050
ξ	0.03024	0.00255
ϵ_h	0.58832	0.96905

3.3 YORP effect computation

The total YORP torque \mathbf{M} resulting from the force (57)

$$\mathbf{M} = \oint \left(\mathbf{r} \times \frac{d\mathbf{F}}{dS} \right) dS, \quad (67)$$

is obtained by integration over the surface of the body. The way the integration is handled depends on the type of body shape model: it can be performed analytically if the surface equation is explicit (e.g. spherical harmonics expansion) or, more often, replaced by the sum over the flat faces of a triangulation mesh. In the Rubincam approximation, when $Q = 0$, we can simply substitute equation (57) into equation (67) to obtain the torque for a given position of the Sun in the body frame. Most often, the resulting torque values are then averaged with respect to rotation and orbital motion in order to extract the secular effects in rotation rate and attitude dynamics. This step requires assumptions about the nominal rotation model that provides the averaging kernel and solar ephemerides.

When the heat conduction is included, the nominal rotation model enters much earlier than in the final averaging: the surface temperature oscillations are lagged with respect to the insolation, and hence we cannot find Q , required by the torque formula, without knowledge of the rotation history. Choosing the simplest principal axis rotation mode (known as the gyroscopic approximation), we can easily add non-Lambertian corrections to the algorithm of Breiter et al. (2010) based on a non-linear one-dimensional thermal model.

The one-dimensional model, where conduction is restricted to the direction normal to the surface, allows a separate treatment of each triangular face of the shape mesh. There, having specified the obliquity ε (the angle between the spin axis and normal to the orbit), we sample the mean anomaly and rotation phase, creating the vector of absorbed radiant flux values (the first term on the right-hand side of equation 43). Its discrete Fourier transform (DFT) serves to compute the DFT spectrum of Q by an iterative process. Once the spectrum of Q is known, we are able to compute the torque \mathbf{M} . Until this step, no essential modifications of the algorithm are required; all we have to do is to replace the constant albedo A (understood as the Bond albedo A_B) in the boundary conditions of Breiter et al. (2010) by the hemispheric albedo function $A_h(\mu_\odot)$. Apart from this point, the heat diffusion solver remains practically unchanged; however, computing the mean torque demands further revision. The spectrum of absorbed power flux $\nu J \mu_\odot (1 - A_h)$, evaluated for the conductivity contribution, cannot be recycled in the Rubincam part, because the hemispheric albedo is not a constant. Thus, outside the conductivity related block, we directly compute the mean values of projections of the Rubincam part $d\mathbf{M}$ (given by equation 64 with $Q = 0$) on unit vectors

$$\begin{aligned} \mathbf{e}_1 &= \sin \Omega' \mathbf{e}_x + \cos \Omega' \mathbf{e}_y, \\ \mathbf{e}_2 &= -\cos \Omega' \mathbf{e}_x + \sin \Omega' \mathbf{e}_y, \\ \mathbf{e}_3 &= \mathbf{e}_z, \end{aligned} \quad (68)$$

where \mathbf{e}_x , \mathbf{e}_y and \mathbf{e}_z form the body-fixed frame basis, and Ω' is the rotation phase measured from the asteroid's equinox (Breiter et al. 2010; N.B. the prime is added to avoid confusion with the solid angle Ω of the present paper). Then we add the mean values resulting from the DFT spectrum of Q , obtaining the final averaged torque projections $\langle M_i \rangle = \langle \mathbf{M} \cdot \mathbf{e}_i \rangle$.

If ω denotes the rotation rate, the dynamics in the gyroscopic approximation is governed by

$$\dot{\omega} = \frac{M_3}{C}, \quad (69)$$

$$\dot{\varepsilon} = \frac{M_1}{\omega C}, \quad (70)$$

$$\dot{\Omega}' = \omega - \frac{M_2}{\omega C \tan \varepsilon}, \quad (71)$$

where C designates the maximum moment of inertia in the principal axes frame.

The conclusion of Breiter et al. (2010), that all one-dimensional thermal models imply the independence of the mean period

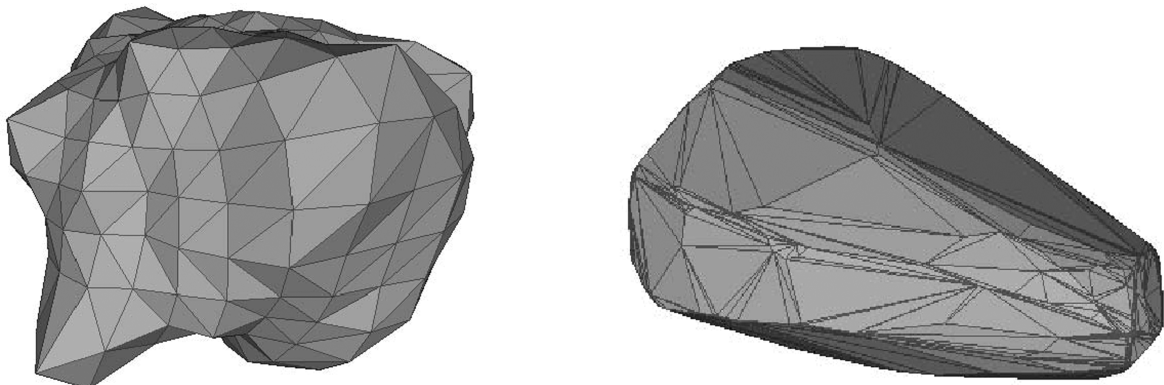


Figure 2. Triangulated shape models: left, (54509) YORP; right, (3103) Eger.

Table 2. Physical and orbital data for the test bodies.

		(54509) YORP	(3103) Eger
Epoch	JD	2452117.5	2446617.0
Semi-axis	au	0.9930	1.4068
Eccentricity		0.2305	0.3548
Inclination	deg	1.9971	20.939
Asc. node	deg	283.835	129.972
Arg. perihelion	deg	272.091	253.661
Rotation period	h	0.2029	5.7102
Ecliptic pole (λ, β)	deg	(180, -85)	(224, -72)
Effective diameter	m	113	1778
Density	kg m^{-3}	2500	2800
Conductivity	$\text{W m}^{-1} \text{K}^{-1}$	0.02	0.02
Specific heat	$\text{J kg}^{-1} \text{K}^{-1}$	680	680
Max. mom. inertia	kg m^2	3.04×10^{12}	2.80×10^{20}

related component $\langle M_3 \rangle$ on conductivity, holds true regardless of the scattering and emission laws.

4 EXEMPLARY RESULTS

In order to see how the improvement of scattering and emission laws affects the simulated YORP effect, we consider two exemplary objects out of the four known to have observationally confirmed spin acceleration: the (54509) YORP asteroid with an irregular, radar-determined shape model³ (Taylor et al. 2007) and (3103) Eger with a convex shape model obtained by light-curve inversion (Durech et al. 2009). Both shape models, consisting of 572 (YORP) and 1972 (Eger) triangular facets, are displayed in Fig. 2. The orbital and physical parameters assumed in our computations are presented in Table 2. Generally, we have tried to maintain coherence with the data applied by Taylor et al. (2007) and Durech et al. (2009). The effective diameter (the radius of a sphere with the same volume as an object) of Eger was selected indirectly; actually, we scaled the asteroid to have the same volume as a spheroid with semi-axes 2.3 and 1.5 km (Benner et al. 1997).

Considering (54509) YORP, we have compared two variants: a realistic assumption that the asteroid is an S-type object with geometric albedo $p = 0.1$, and a fictitious case of spectral type E with $p = 0.6$. The Hapke parameters are taken from Table 1. If the Lambert model is assumed, the appropriate Bond albedo and emissivity from Table 1 are applied. For the Lommel–Seeliger model, the single scattering albedo w is computed from A_B according to equation (A3) and the emissivity follows from $\epsilon_h = 1 - A_B$. Of course, the Lommel–Seeliger scattering is not considered for $p = 0.6$, which might lead to hemispheric albedo values outside the $[0, 1]$ interval.

Fig. 3 presents the simulation results for (54509) YORP. Although its caption mentions only the Lambert and Hapke models, the Lommel–Seeliger results for $p = 0.1$ are still there; these practically coincide with the Lambertian solid line. We have traced the values of $\langle M_i \rangle$ for all possible obliquities ϵ , although the actual value for (5409) YORP is $\epsilon = 173^\circ$. The angle between the asteroid’s vernal equinox and the orbital perihelion is $\omega_0 = 102^\circ$, and we used this value for all epsilon values in Fig. 3. The value of ω_0 is irrelevant

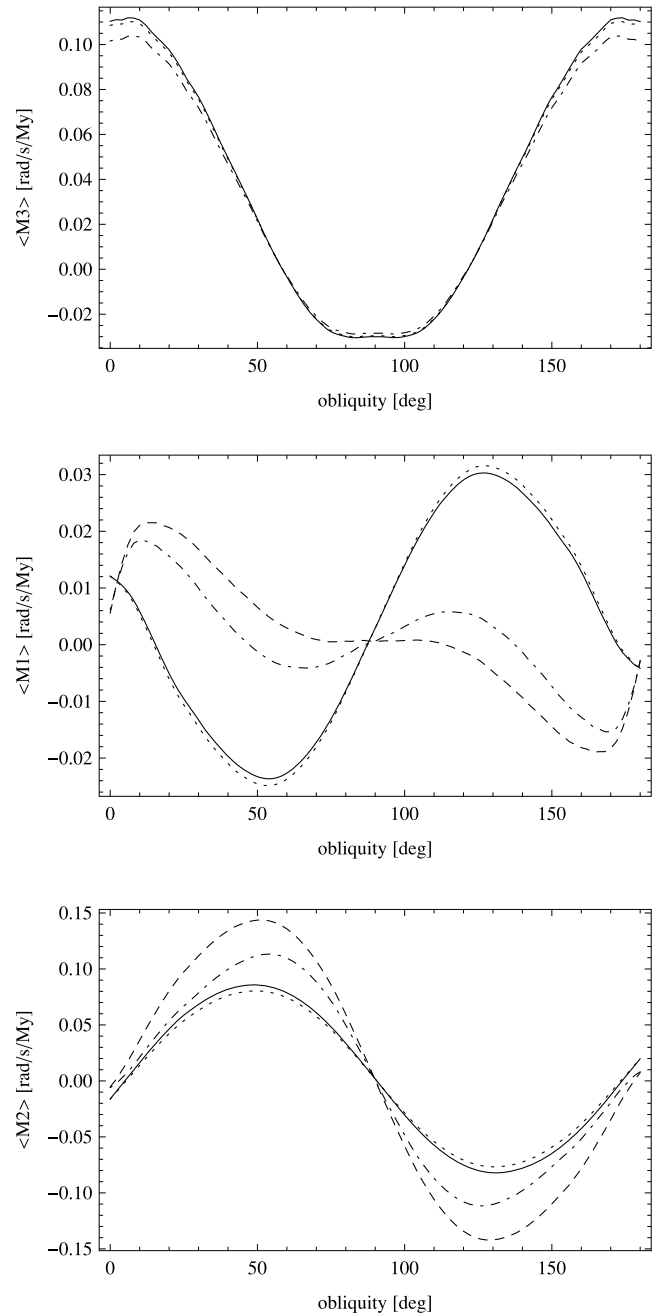


Figure 3. Secular YORP effect components on (54509) YORP: solid line, Lambert type S; dotted, Hapke type S ($p = 0.1$); dashed, Lambert type E; dot-dashed, Hapke type E ($p = 0.6$).

for $\langle M_3 \rangle$, governing the evolution of rotation period, but essential from the point of view of $\langle M_1 \rangle$ and $\langle M_2 \rangle$, responsible for the attitude (Breiter et al. 2010). Considering $\langle M_3 \rangle$ values (Fig. 3, top), we observe that, in spite of the irregular shape, the type of scattering model at low $p = 0.1$ has practically no influence on the YORP effect in the rotation period, and even at the high albedo case ($p = 0.6$) the difference between the Lambert and Hapke models does not exceed 10 per cent. The situation is different for $\langle M_1 \rangle$ and $\langle M_2 \rangle$, but there, even for the Lambert model, we have a dependence on albedo resulting from the heat conduction. Although, for $p = 0.1$, there is almost no difference between the Lambert, Lommel–Seeliger and type S Hapke models, a high geometric albedo $p = 0.6$ leads to

³ More precisely, we use the ‘A-Rough’ model available through the National Aeronautics and Space Administration (NASA) Planetary Data System (PDS) website, <http://pds.jpl.nasa.gov/>.

Table 3. Mean YORP torques for (54509) YORP at $\varepsilon = 173^\circ$ and $\omega_0 = 102^\circ$. All values in 10^{-16} rad s $^{-2}$.

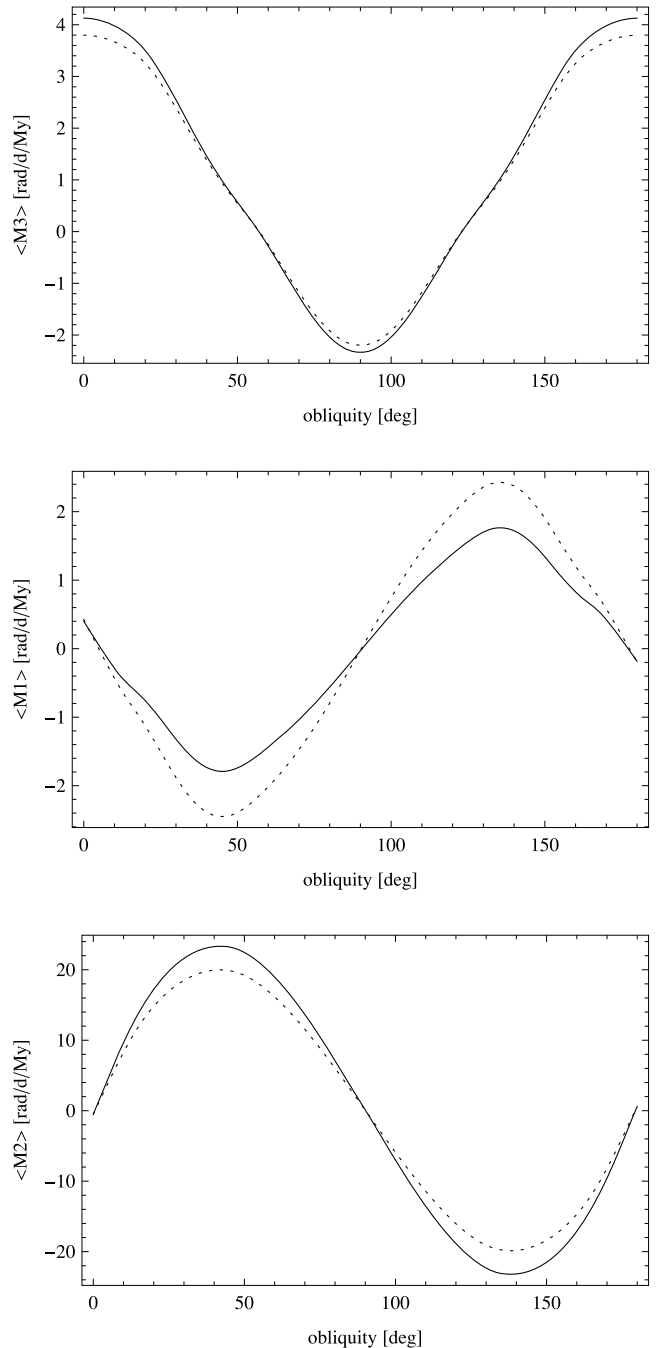
		$\langle M_1 \rangle$	$\langle M_2 \rangle$	$\langle M_3 \rangle$
Lambert	$p = 0.1$	-0.21	-0.92	35.5
Lommel–Seeliger	$p = 0.1$	-0.18	-0.46	35.4
Hapke (type S)	$p = 0.1$	-0.07	-0.34	34.9
Lambert	$p = 0.6$	-5.07	-6.41	35.5
Hapke (type E)	$p = 0.6$	-4.44	-2.82	32.9

significant differences between the Lambert approximation (dashed line) and the E-type Hapke model (dot-dashed line). The results for the nominal values of $\varepsilon = 173^\circ$ and $\omega_0 = 102^\circ$ are collected in Table 3. Comparing $\langle M_3 \rangle$ with the observed $\dot{\omega} = (4.7 \pm 0.5) \times 10^{-16}$ rad s $^{-2}$ (Taylor et al. 2007), we note that the present model overestimates $\dot{\omega}$ almost 7.6 times (i.e. more than the relevant models used in Taylor et al. 2007). However, the most significant part of this increase is a result of the recomputed reduction to the centre of mass and (more important) principal axes system. If the original body fixed frame is used, we obtain a lower factor of 7.0.

In the simulations referring to (3103) Eger, we have compared only the Lambert model and the Hapke model for spectral type E with a high geometric albedo $p = 0.6$ (Fig. 4). In spite of a convex shape, excluding all shadowing effects, the dependence of all three $\langle M_i \rangle$ components on the scattering/emission model has the same relative magnitude as in the case of (54509) YORP. The values for the actual spin axis orientation of Eger are provided in Table 4. Interestingly, our modelled values of $\langle M_3 \rangle$ are very close to the observed $\dot{\omega} = (1.2 \pm 0.8) \times 10^{-18}$ rad s $^{-2}$ reported by Āurech et al. (2009). Of course, this exceptional agreement could be a lucky coincidence, recalling the inaccurate nature of the photometric convex shape model, the roughly estimated density and the still large error margin of the $\dot{\omega}$ determination.

5 CONCLUSIONS

As far as the photometry of Solar system bodies is concerned, the bidirectional reflectance model elaborated by Hapke leads to significantly different results from the basic Lambertian framework. The YORP effect in the rotation period seems to be almost insensitive to the scattering/emission model and even at the highest observed albedo values the difference between the two models does not increase to more than 10 per cent. However, this low sensitivity should not be interpreted as evidence of the insensitivity of the scattered radiation torque on the reflectivity model. Actually, the situation is quite the opposite. Even for a given Bond albedo value, the part of the YORP torque originating from the recoil of reflected light significantly depends on the form of the BRDF. However, the conservation of energy implies that, in the absence of conductivity, the sum of scattered and thermally reradiated energy is always equal to the incident energy. If the hemispheric albedo in some reflection model is higher than the Bond albedo of the Lambert case, more power is scattered, but also less power is thermally re-emitted, and vice versa (see Fig. 5). Actually, the same mechanism of energy balance is responsible for the independence of the YORP effect from the albedo and emissivity in the traditional Rubincam approximation with Lambertian scattering/emission. In the one-dimensional thermal model considered in this paper, the $\langle M_3 \rangle$ component behaves exactly as in the Rubincam approximation. So, the dependence on reflectance is only a result of secondary effects – mostly related

**Figure 4.** Secular YORP effect components on (3103) Eger: solid line, Lambert type E; dotted, Hapke type E ($p = 0.6$).**Table 4.** Mean YORP torques for (3103) Eger at $\varepsilon = 177^\circ$ and $\omega_0 = 100^\circ$. All values in 10^{-18} rad s $^{-2}$.

		$\langle M_1 \rangle$	$\langle M_2 \rangle$	$\langle M_3 \rangle$
Lambert	$p = 0.6$	0.002	-0.93	1.51
Hapke (type E)	$p = 0.6$	0.015	-0.77	1.39

to the small deviation of the recoil force from the normal to the surface.

Using a more elaborate scattering method is more important in the part of the YORP effect responsible for the orientation of the

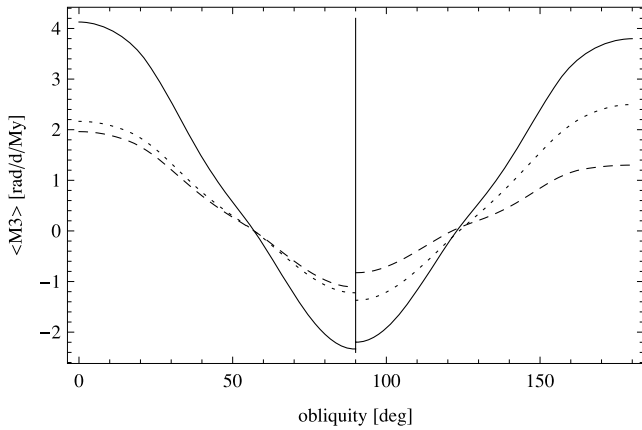


Figure 5. YORP effect in ω and its components for (3103) Eger: dashed line, scattered light; dotted line, thermal radiation; solid line, total. The Lambert case is shown on the left, compared with the Hapke model (right).

spin axis. In the Rubincam approximation, the situation is similar to that of $\langle M_3 \rangle$. However, the Rubincam approximation itself is definitely unrealistic for the attitude, even at moderate values of conductivity. The influence of heat conduction is proportional to the absorbed fraction of incident energy, and hence to the albedo. This means that two scattering models with different dependence of hemispheric albedo on the Sun’s zenith distance will differently affect the balance between scattered and reradiated power. This explains why using the Hapke BRDF instead of the Lambertian model is more important for $\langle M_1 \rangle$ and $\langle M_2 \rangle$, than for $\langle M_3 \rangle$.

ACKNOWLEDGMENTS

The work of SB was supported by the Polish Ministry of Science and Higher Education (grant No N203 302535). The work of DV was supported by the Czech Grant Agency (grant 205/08/0064) and the Research Programme MSM 0021620860 of the Czech Ministry of Education.

REFERENCES

- Benner L. A. M. et al., 1997, *Icarus*, 130, 296
 Bowell E., Hapke B., Domingue D., Lumme K., Peltoniemi J., Harris A. W., 1989, in Binzel R. P., Gehrels T., Matthews M. S., eds, *Asteroids II*. Univ. Arizona Press, Tuscon, AZ, p. 524
 Breiter S., Michalska H., Vokrouhlický D., Borczyk W., 2007, *A&A*, 471, 345
 Breiter S., Bartczak P., Czekaj M., Oczujda B., Vokrouhlický D., 2009, *A&A*, 507, 1073
 Breiter S., Bartczak P., Czekaj M., 2010, *MNRAS*, in press (doi: 10.1111/j.1365-2966.2010.17223.x)
 Chandrasekhar S., 1950, *Radiative Transfer*. Clarendon, Oxford
 Chesley S. R. et al., 2003, *Sci*, 302, 1739
 Čuk M., Burns J. A., 2005, *Icarus*, 176, 418
 Ďurech J. et al., 2008a, *A&A*, 488, 345
 Ďurech J. et al., 2008b, *A&A*, 489, L25
 Ďurech J. et al., 2009, *AAS Division for Planetary Sciences Meeting Abstracts*, 41, 56.04
 Fairbairn M. B., 2005, *J. Royal Astron. Soc. Canada*, 99, 92
 Hapke B., 1981, *J. Geophys. Res.*, 86, 4571
 Hapke B., 1984, *Icarus*, 59, 41

- Hapke B., 1986, *Icarus*, 67, 264
 Hapke B., 1993, *Theory of Reflectance and Emittance Spectroscopy*. Cambridge Univ. Press, Cambridge
 Hapke B., 2002, *Icarus*, 157, 523
 Hapke B., 2008, *Icarus*, 195, 918
 Hapke B., Wells E., 1981, *J. Geophys. Res.*, 86, 3055
 Kaasalainen M., Ďurech J., Warner B. D., Krugly Y. N., Gaftonyuk N. M., 2007, *Nat*, 446, 420
 Lagerros J. S. V., 1996, *A&A*, 310, 1011
 Lagerros J. S. V., 1998, *A&A*, 332, 1123
 Lebofsky L. A., Spencer J. R., 1989, in Binzel R. P., Gehrels T., Matthews M. S., eds, *Asteroids II*. Univ. Arizona Press, Tuscon, AZ, p. 128
 Lowry S. C. et al., 2007, *Sci*, 316, 272
 Lumme K., Bowell E., 1981, *AJ*, 86, 1694
 McMahon J., Scheeres D., 2010, *Celest. Mech. Dyn. Astron.*, 106, 261
 Nesvorný D., Vokrouhlický D., 2008, *A&A*, 480, 1
 O’Keefe J. A., 1976, *Tektites and Their Origin*. Elsevier, Amsterdam
 Paddack S. J., 1969, *J. Geophys. Res.*, 74, 4379
 Radzievskii V. V., 1954, *Dokl. Akad. Nauk SSSR*, 97, 49
 Rubincam D. P., 2000, *Icarus*, 148, 2
 Rubincam D. P., Paddack S. J., 2010, *Icarus*, 209, 863
 Scheeres D. J., 2007, *Icarus*, 188, 430
 Scheeres D. J., Gaskell R. W., 2008, *Icarus*, 198, 125
 Statler T. S., 2009, *Icarus*, 202, 502
 Taylor P. A. et al., 2007, *Sci*, 316, 274
 Verbiscer A. J., Veveřka J., 1995, *Icarus*, 115, 369
 Vokrouhlický D., Bottke W. F. Jr, 2001, *A&A*, 371, 350
 Vokrouhlický D., Chesley S. R., Matson R. D., 2008, *AJ*, 135, 2336
 Yarkovsky I. O., 1901, *The density of luminiferous ether and the resistance it offers to motion* (in Russian), Tipografiadina Bryansk

APPENDIX A: LOMMEL–SEELIGER APPROXIMATION

The Lommel–Seeliger scattering law (Fairbairn 2005) is defined by the BRDF

$$f_{\text{LS}}(s, \theta) = \frac{w}{4\pi(\mu_{\odot} + \mu)}, \quad (\text{A1})$$

which can be seen as a simplified Hapke model independent of the phase angle g . Using this simple law, we find most of the expressions in an exact, closed form, depending on the single scattering albedo w . The hemispheric albedo is

$$A_{\text{h}}(\mu_{\odot}) = \frac{w}{2} \left(1 + \mu_{\odot} \ln \frac{\mu_{\odot}}{1 + \mu_{\odot}} \right), \quad (\text{A2})$$

leading to the Bond albedo

$$A_{\text{B}} = \frac{2(1 - \ln 2)}{3} w \approx 0.204569w, \quad (\text{A3})$$

and the geometric albedo

$$p = \frac{w}{8}. \quad (\text{A4})$$

Note that equation (A4) leads to problems with $w > 1$ in the Hapke thermal radiation expressions if we try to use it for bright objects with $p > 0.125$. In these circumstances, we combine the Lommel–Seeliger scattering with a Lambertian grey-body emission model, imposing $\xi = 0$. Then,

$$X_1(\mu_{\odot}) = \frac{w\mu_{\odot}}{12} \left[1 + 6\mu_{\odot} + 2\mu_{\odot}(2 + 3\mu_{\odot}) \ln \frac{\mu_{\odot}}{1 + \mu_{\odot}} \right] \quad (\text{A5})$$

and $X_2 = 0$. The resulting force per area

$$\frac{d\mathbf{F}}{dS} = -\frac{2}{3c}[vJ\mu_{\odot} + Q]\mathbf{n} + \frac{vJ}{c}X_1\mathbf{n} \quad (\text{A6})$$

is directed along the surface normal, similarly to the Lambertian case.

APPENDIX B: DIRECT RADIATION PRESSURE

In the usual YORP models of a single object orbiting the Sun, the direct radiation pressure, opposite to the Sun's vector \mathbf{s} , is either a priori discarded or its effect disappears after the double (rotation and orbit) averaging. However, this phenomenon may play some role when a binary system is studied – most notably for the BYORP effect (Ćuk & Burns 2005; McMahon & Scheeres 2010). In such cases, the force and torque should be complemented with the following terms:

$$\frac{d\mathbf{F}_d}{dS} = -\frac{vJ\mu_{\odot}}{c}\mathbf{s} = -\frac{vJ\mu_{\odot}}{c}(\mu_{\odot}\mathbf{n} + s_{\odot}\mathbf{m}), \quad (\text{B1})$$

which is the addition to equation (57), and the resulting torque

$$\frac{d\mathbf{M}_d}{dS} = \mathbf{r} \times \frac{d\mathbf{F}_d}{dS}. \quad (\text{B2})$$

Note that for a binary system the visibility function v additionally involves occultations by the second object.

With these complements, the complete force $d\mathbf{F}_c = d\mathbf{F} + d\mathbf{F}_d$ acting on a surface element is

$$d\mathbf{F}_c = -\frac{2}{3}\frac{1+\xi}{c}[vJ\mu_{\odot} + Q]dS + \frac{vJ}{c} \times \left[(X_1 - \mu_{\odot}^2) dS - (X_2 + \mu_{\odot} s_{\odot}) \mathbf{m} dS \right], \quad (\text{B3})$$

and the complete torque is readily obtained by the cross product

$$d\mathbf{M}_c = \mathbf{r} \times d\mathbf{F}_c. \quad (\text{B4})$$

Equation (B1) involves an implicit statement that all photons hitting the surface are absorbed and transfer their momentum before being re-emitted in any form, including the one called reflection. In a perfect specular reflection, all photons arriving from $\mathbf{s} = \mu_{\odot}\mathbf{n} + s_{\odot}\mathbf{m}$, leave the surface in the symmetric direction $\mathbf{s}' = \mu_{\odot}\mathbf{n} - s_{\odot}\mathbf{m}$. So, the total effect of perfect specular reflection is

$$d\mathbf{F}_s = -\frac{2vJ\mu_{\odot}^2}{c}dS, \quad (\text{B5})$$

with the \mathbf{m} component cancelled. As a consequence, we can interpret the occurrence of function X_2 as a footprint of imperfect specular reflection in the Hapke model, with only a part of the power incoming from \mathbf{s} leaving the surface along \mathbf{s}' .

This paper has been typeset from a $\text{\TeX}/\text{\LaTeX}$ file prepared by the author.